Voltage Profile along the Permeation Pathway of an Open Channel

Jorge E. Contreras,[†*] Jin Chen,[†] Albert Y. Lau,[‡] Vishwanath Jogini,[‡] Benoît Roux,[‡] and Miguel Holmgren[†*]
[†]Molecular Neurophysiology Section, Porter Neuroscience Research Center, National Institute of Neurological Disorders and Stroke, National Institutes of Health, Bethesda, Maryland; and [‡]Department of Biochemistry and Molecular Biology, The University of Chicago, Chicago, Illinois

ABSTRACT For ion channels, the transmembrane potential plays a critical role by acting as a driving force for permeant ions. At the microscopic level, the transmembrane potential is thought to decay nonlinearly across the ion permeation pathway because of the irregular three-dimensional shape of the channel's pore. By taking advantage of the current structural and functional understanding of cyclic nucleotide-gated channels, in this study we experimentally explore the transmembrane potential's distribution across the open pore. As a readout for the voltage drop, we engineered cysteine residues along the selectivity filter and scanned the sensitivity of their modification rates by Ag^+ to the transmembrane potential. The experimental data, which indicate that the majority of the electric field drops across the selectivity filter, are in good agreement with continuum electrostatic calculations using a homology model of an open CNG channel. By focusing the transmembrane potential across the selectivity filter, the electromotive driving force is coupled with the movement of permeant ions in the filter, maximizing the efficiency of this process.

INTRODUCTION

Ions cross biological membranes through specialized integral membrane proteins known as ion channels (1) and transporters (2). Ion channels allow the passage of ions at rates $>10^7$ ion/s (1,3). These high throughput rates are determined by a variety of physical factors, such as the shape of the permeation pathway, the intrinsic electrostatic potential of the protein along the permeation pathway, ion-ion interactions within the pore, and the transmembrane potential itself (1). In the last 10 years, the increasing availability of high-resolution ion-channel crystal structures, together with functional and computational studies, has permitted a more microscopic account of how some of these parameters influence permeation (4–19). The transmembrane potential has been studied mostly using computational approaches, remaining elusive to direct experimentation. A continuum electrostatic approximation leading to a modified Poisson-Boltzmann equation was developed to describe the influence of the transmembrane potential on transmembrane proteins (i.e., the PB-V equation) (15). Calculations based on crystal structures and homology models of potassium channels suggested that the transmembrane voltage in an open channel is mainly focused along the narrow selectivity filter (11,12,20). Although this concept is in broad accord with voltage-dependent current block by specific ions and organic molecules (21–25), physical interpretations from these studies have been difficult. In some instances, either multiion occupancy and/or the intrinsic voltage dependence of channel gating contribute to the voltage dependence of blockade. Furthermore, the precise locations of where these blockers act along the permeation pathway are difficult to pinpoint.

In this study, we determine the voltage profile along an open cyclic nucleotide-gated (CNG) channel by substituting cysteine at three positions known to line the permeation pathway (26,27): the intracellular cavity, and the inward and outward facing ends of the selectivity filter. We then evaluate the voltage dependence of modification by positively charged thiol reagents such as Ag^+, Cd^{2+}, and trimethylaminoethyl methanethiosulfonate (MTSET). Similar to permeant ions, these probes will sense the transmembrane voltage as they transverse the permeation pathway. Therefore, changes in the reaction kinetics between these thiol reagents and the substituted cysteines can be used to infer the voltage profile along the pore. By comparing the voltage dependence of the apparent modification rates along the permeation pathway of CNG channels, we determined that, as hypothesized, the voltage drops exclusively along the selectivity filter in an open channel. These experimental observations are consistent with electrostatic PB-V calculations performed on a homology model of an open CNG channel based on the high-resolution structure of the NaK channel (28).

MATERIAL AND METHODS

Mutagenesis and expression

Cysteine mutations were introduced in a cysteine-free CNGA1 channel, a kind gift from William Zagotta (University of Washington, Seattle, WA). All mutations were generated by standard PCR techniques and verified by DNA sequencing. In vitro cRNA synthesis was performed with a T7 promoter-based kit from Ambion (Austin, TX). cRNA was injected into *Xenopus* oocytes and allowed to express for 3–5 days before electrophysiological recordings.

Electrophysiology

Ionic currents were measured from inside-out excised patches (29) using an Axopatch 200B amplifier (Axon Instruments, Foster City, CA). Bath

Submitted April 15, 2010, and accepted for publication August 26, 2010.

*Correspondence: holmgren@ninds.nih.gov or contrerjo@ninds.nih.gov

Editor: Richard W. Aldrich.

0006-3495/10/11/2863/7 $2.00

doi: 10.1016/j.bpj.2010.08.053

solutions were rapidly exchanged by a computer-controlled system (RSC-200; Biologic Science Instruments, Knoxville, TN). Bath and pipette solutions containing 120 mM of either NaCl or $NaNO_3$ (when silver ions were used), 10 mM HEPES, and EDTA (pH = 7.4). For experiments using MTSET the [EDTA] was 0.2 mM. EDTA was omitted in experiments using Cd^{2+} and extracellular Mg^{2+}. Solutions used in experiments with Ag^{+} contained 10 mM EDTA to buffer free Ag^{+} to a desired concentration (26). Cd^{2+} modification experiments in the presence of 40 mM external Na^{+} were performed by reducing the concentration of Na^{+} without compensating for ionic strength or the change in osmolarity because we have not been able to find a suitable replacement that is nonpermeant. Large cations like NMDG or arginine, and osmotic substitutes like sucrose, interact with the external mouth of CNG channels, causing substantial block at all voltages (see Fig. S1 in the Supporting Material).

Molecular modeling

Sequence alignment of CNGA1 (GI: 27805875) with NaK (GI: 30018851) was performed as previously described (27). The side chains of the CNG channel were substituted onto the main chain of the open NaK channel's crystal structure (28) (PDB: 3E86) using SCWRL (30). Only the M1-P-M2 region was modeled. The loop region between the M1 and P helices (residues 359–365) was rebuilt using ModLoop (31) because NaK has fewer residues in this region. Protein side chains and the rebuilt loop were refined by energy minimization and molecular dynamics simulations using CHARMM (32). All main chain atoms except residues 330–346 (the C-terminal end of the M1 helix and the connecting loop) and 365–369 (the loop between the filter and the M2 helix) were constrained during refinement.

Calculation of the transmembrane potential

The fraction of transmembrane potential was calculated from the CNG model using the modified Poisson-Boltzmann (PB-V) equation (15) implemented in the finite-difference PBEQ module (33) of CHARMM (32). Similar calculations carried out for the KcsA channel have been previously described (12,20) and experience shows that the results are not highly sensitive to the details of the model. A dielectric of 2 was assigned to the protein. The membrane was represented as a 25 Å slab with a dielectric of 2. The bulk solvent on either side of the membrane, and the aqueous crevices of the pore, were assigned a dielectric of 80. A water probe of 1.4 Å radius was used to define the molecular surface corresponding to the dielectric boundary, using a 0.5 Å grid (33). It should be noted that all protein charges were turned off for the calculation of the membrane potential profile, as prescribed by the PB-V theory (15).

RESULTS

Voltage drop along the intracellular cavity

To estimate the voltage landscape along the permeation pathway of an open channel, we used small probes (34–36), which were driven by voltage toward specific sulfhydryl side chains substituted along the pore (Fig. 1). This approach allowed us to define the precise location of the target sites. It is feasible only under conditions when the channel's gating is not sensitive to voltage, as for CNG channels in the presence of saturating concentrations of cGMP (37) (see also Fig. S2). Fig. 2 *A* shows the experimental strategy used to examine channel activity before and after chemical modification. In each experiment, inside-out patches with multiple CNG channels were

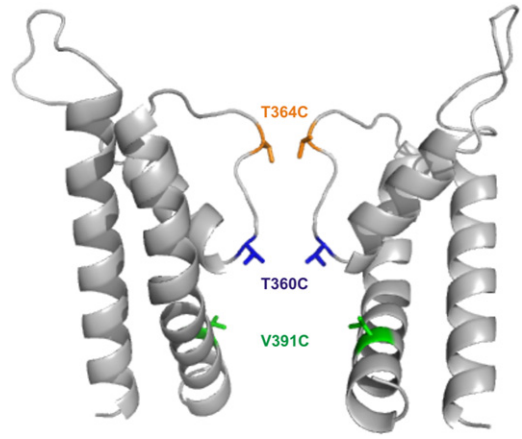

FIGURE 1 Homology model of the CNG channel pore in the open conformation. The pore model includes segments S5 and S6 of the CNGA1 channel. For simplicity, only two opposite subunits are shown. The homology model of the CNG pore was built using the structure of an open NaK channel as template (28). This bacterial channel has been proposed to resemble the ion permeation pathway of CNG channels (27). Residues that were substituted by cysteine in CNG channels are highlighted in colors that will be conserved throughout the article.

positioned in front of a perfusion change system that allowed rapid changes of the internal solution. The membrane potential was held at 0 mV, except during treatments when channels were exposed to a two-second application of a specific cysteine reagent at a defined voltage, and with a saturating concentration of agonist. The ionic current through CNG channels before and after modification was assessed with two brief 50-ms depolarizations to +60 mV: one in the absence, and one in the presence, of 2 mM cGMP. Subtraction of these currents yielded the cGMP-activated current. Fig. 2 *B* shows leak-subtracted current records before (*black*) and after (*green*) four successive MTSET treatments on V391C mutant channels at a membrane potential of −40 mV (*green traces*). At this position, located in the middle of the intracellular cavity, chemical modification by the positively charged MTS reagent produced a complete and irreversible current reduction. The time course of MTSET modification was similar at −40 and 40 mV (Fig. 2 *C*). The apparent second-order MTSET modification rates were estimated from the reciprocal of the time constant obtained by single exponential fits to the current reduction data and the concentration of reagent applied. The apparent modification rates for MTSET were similar for voltages from −60 to 60 mV (Fig. 2 *D*). Similarly, modification rates did not differ with voltage when V391C channels were exposed to Cd^{2+} (Fig. 2 *E*). These results suggest that positively charged probes sense no portion of the transmembrane potential as they move from the intracellular bulk solution to the middle of the intracellular cavity.

From our previous work (26), we know that Ag^{+} is the only cysteine reagent that can access the entire selectivity filter of CNG channels, perhaps because it is a small monovalent

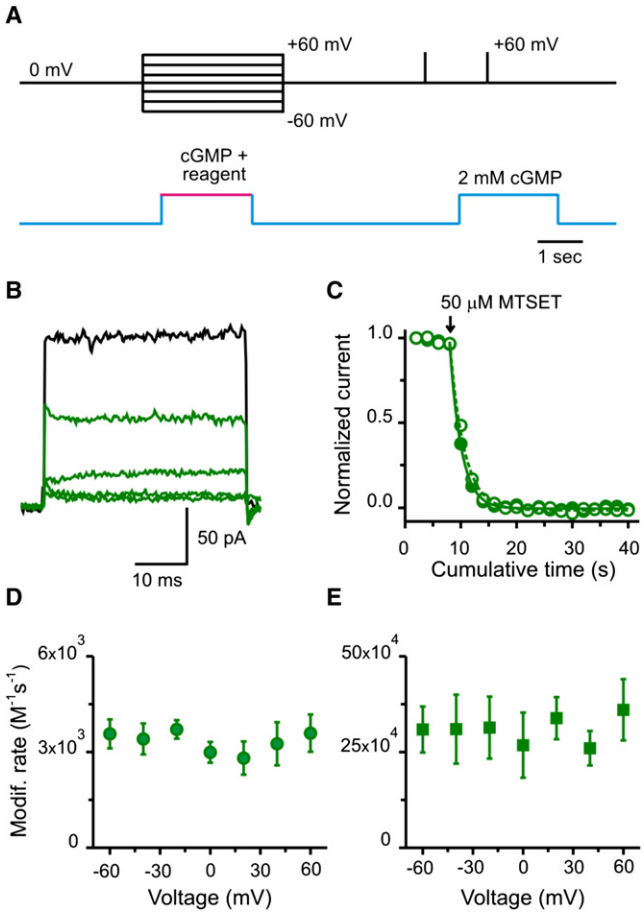

FIGURE 2 Modification at position V391C: the middle of the intracellular cavity. (*A*) Experimental protocol to estimate modification rates at different voltages. In each experiment, chemical modification was performed using 2 s treatments at a define voltage and under saturating [cGMP] (2 mM). Subsequently, cGMP-activated currents were monitored by subtracting a 50-ms pulse to +60 mV in the absence of cGMP from a similar pulse in the presence of 2 mM cGMP. Treatments were applied every 15 s. (*B*) cGMP-activated current traces before (*black trace*) and after four consecutive MTSET treatments (*green traces*). (*C*) Time course of MTSET modification. Plot shows normalized current upon MTSET applications (*arrow*) at −40 (*open green circles*) and 40 mV (*solid green circles*), respectively. Dashed (−40 mV) and solid (40 mV) lines represent single exponential fits to the cumulative modification data at each voltage. *(D)* Voltage dependence of the modification rate for MTSET. The concentrations of MTSET used in these experiments were 50 or 100 μM. $n = 20$ patches. (*E*) Voltage dependence of the modification rate for Cd^{2+}. These apparent rates were estimated with [Cd^{2+}] between 0.5 and 2 μM. $n =$ 27 patches.

cation, like Na^+ or K^+. At position T360C, located at the intracellular end of the selectivity filter (i.e., at the top of the intracellular cavity), the time courses for Ag^+ modification were almost indistinguishable between −40 and 40 mV (Fig. 3 *A*). The apparent modification rates for voltages between −60 and 60 mV were similar, being slightly slower at the most negative voltage (Fig. 3 *B*; *solid symbols*). The lack of significant voltage dependence suggests that the voltage drop along the intracellular cavity of the channel is

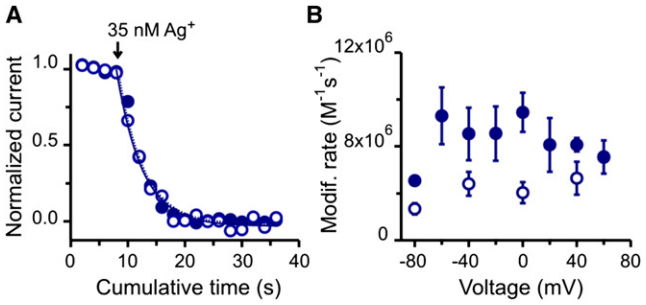

FIGURE 3 Modification at position T360C: the internal end of the selectivity filter facing the intracellular cavity. (*A*) Time course of Ag^+ modification. (*Open* and *solid blue symbols*) Two experiments in which modification was assessed at −40 mV and 40 mV, respectively. (*Lines*) Single exponential fits to the cumulative modification at −40 (*dashed*) and 40 mV (*solid*). (*B*) Voltage dependence of Ag^+ modification in the absence (*solid symbols*; $n = 28$ patches) and presence (*open symbols*; $n = 23$ patches) of 50 μM external Mg^{2+}. All apparent rates were estimated with 35 nM Ag^+.

negligible. However, it is possible that a sizeable voltage drop along this region is being masked by Ag^+ permeation to the outside. In other words, occupancy at the site of modification appears voltage-independent because access from the inside and exit to the outside, both voltage dependent transitions, have similar magnitudes. To explore this possibility, we performed Ag^+ modifications in the presence of 50 μM extracellular Mg^{2+}, which is known to block permeation by interacting with the external end of the selectivity filter in a voltage-dependent manner (27,38,39), a property that is preserved in T360C mutant channels (Fig. S3). The presence of external Mg^{2+} slightly slowed the apparent modification rates, without affecting their voltage independence (Fig. 3 *B*; *open symbols*). These results suggest that an intracellular permeant ion will not sense a significant voltage drop as it approaches the intracellular end of the selectivity filter.

Voltage drop across the selectivity filter

In contrast to the results presented thus far, access of intracellularly applied Ag^+ to T364C, a position at the outer end of the selectivity filter (Fig. 1), showed substantial voltage dependence. Fig. 4 *A* illustrates the time courses by Ag^+ modification at −80 (*open circles*), −40 (*semisolid circles*), and 40 mV (*solid circles*). Clearly, they are slower at more negative potentials. A more extensive study of the voltage dependence reveals that the apparent second-order rates approach zero at negative potentials and reach a maximum at positive voltages (Fig. 4 *B*). To analyze these data we consider the following kinetic scheme:

$$S_1 \cdot Ag \underset{}{\overset{K(V)}{\longleftrightarrow}} S_2 \cdot Ag \longrightarrow T364C\text{-}Ag.$$

The model assumes that modification at T364C is preceded by intracellular Ag^+ dwelling between two bound states:

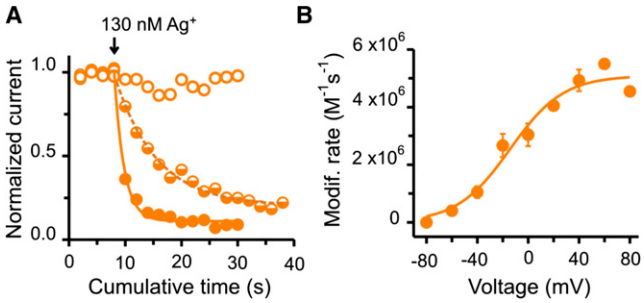

FIGURE 4 Modification at position T364C: the external end of the selectivity filter. (*A*) Time course of Ag^+ modification. Open, semisolid, and solid orange symbols represent three experiments in which apparent modification rates were estimated at −80 mV, −40 mV, and 40 mV, respectively. Lines represent single exponential fits to the cumulative modification at −40 (*dashed*) and 40 mV (*solid*). (*B*) Voltage dependence of the modification rates. The concentrations of Ag^+ used in these experiments were between 75 and 130 nM. Modification rate at −80 mV was set to zero because there was no apparent modification over the timescale used in our protocol. (*Solid line*) Boltzmann fit to the apparent modification rates with an apparent valence of 1.1 ± 0.3 and a midpoint of −14 ± 6 mV. $n = 32$ patches.

$S_1 \cdot Ag$ and $S_2 \cdot Ag$. The state $S_1 \cdot Ag$ might represent a silver ion occupying the intracellular cavity. The $S_2 \cdot Ag$ state would occur in the immediate vicinity of 364C. The $S_1 \cdot Ag \leftrightarrow S_2 \cdot Ag$ transition is at equilibrium and is the sole source of voltage dependence. Finally, Ag^+ interacts irreversibly with the cysteine at position T364C (T364C-Ag) in a voltage-independent manner, with rates that are slower than the preceding transition. In this model, the rate of modification becomes proportional to the occupancy of $S_2 \cdot Ag$, which is distributed with voltage following a Boltzmann relation (Fig. S4 shows a simulation of this model). The solid line in Fig. 4 *B* represents a fit of the modification data to this model. The steepness of the fit is consistent with the movement of a single positive charge across the entire transmembrane potential (i.e., a single Ag^+ senses the entire voltage drop across the membrane when moving from $S_1 \cdot Ag$ to $S_2 \cdot Ag$).

Influence of external ions on modification of cysteines at the intracellular end of the selectivity filter

For almost 40 years it has been known that external ions can cross the pore of voltage-activated potassium channels and influence molecules, such as quaternary ammonium blockers, bound at the intracellular side of the permeation pathway (21,40). This phenomenon has also been observed in CNG channels (41,42). Therefore, in principle, we would expect that external ions permeating through the open CNG channel pore could influence the modification rate of our voltage sensing probes, particularly at negative potentials where the net flux of cations is inward. It is puzzling then that external ions did not appear to affect the voltage dependence of chemical modification, particularly at the internal entryway of the selectivity filter (position T360C). A plausible explanation would be that an external permeant ion (e.g., Na^+) would influence the voltage dependence of modification by an intracellularly applied probe only if that ion displaces the probe from a binding site within the pore. Perhaps, over the voltage range that we explored, the residence time of Ag^+ within the CNG permeation pathway is too short, rendering the interactions between external Na^+ and Ag^+ undetectable.

Intracellular Cd^{2+} can also access the intracellular end of the selectivity filter (position T360C) with modification rates that are 3–4 orders-of-magnitude slower than those measured for Ag^+ (26). We wondered if the residence times of Cd^{2+} in the permeation pathway would be sufficiently slow to detect a voltage dependence to chemical modification imparted from external permeant ions. Fig. 5 *A* shows the time courses of modification by 50 μM internal Cd^{2+} at −60 (*open circles*), 0 (*semisolid circles*), and +60 mV (*solid circles*). In contrast to our observations with Ag^+ (Fig. 3), modification rates with Cd^{2+} at T360C were slowed at negative potentials. A complete study of the apparent

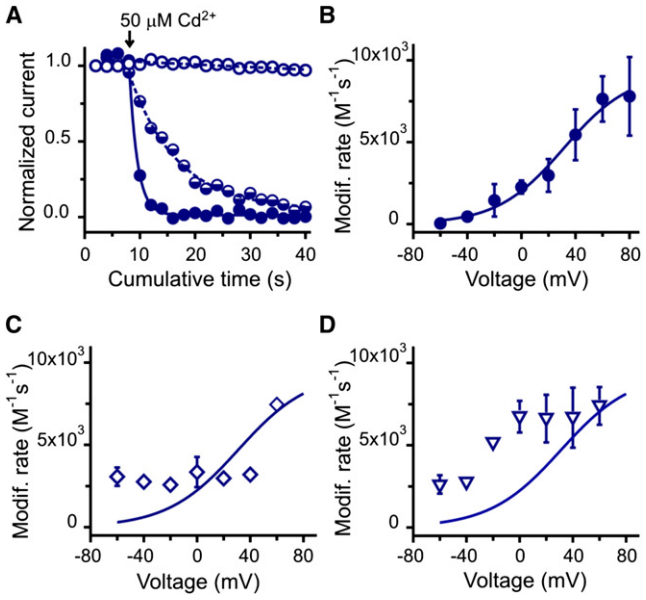

FIGURE 5 Voltage-dependent access of Cd^{2+} to position T360C: effect of extracellular permeant ions. (*A*) Temporal course for Cd^{2+} modification with 50 μM applications as indicated (*arrow*). (*Open*, *semisolid*, and *solid blue symbols*) Three experiments where modification was assessed at −60, 0, +60 mV, respectively. (*Lines*) Single exponential fits to the cumulative modification at each voltage. (*B*) Voltage dependence of modification rates for T360C from −60 mV to +80 mV. (*Solid line*) Boltzmann equation fit of the apparent modification rate with an apparent valence of 1.02 ± 0.2 and a midpoint of 31 ± 8.3 mV. $n = 27$ patches. (*C*) Voltage dependence of the apparent modification rates with Cd^{2+} in the presence of 50 μM external Mg^{2+} (*open diamonds*). $n = 18$ patches. (*D*) Voltage dependence of the apparent modification rates with Cd^{2+} in a 40 mM extracellular Na^+ solution (*open triangles*). $n = 21$ patches. For comparison, the fit from panel *B* is also shown in panels *C* and *D*.

Cd^{2+} modification rates' voltage dependence is shown in Fig. 5 *B*. These rates approach zero at negative voltages and tend to a maximum at positive potentials.

If the voltage dependence of modification originates from the effective displacement of internal Cd^{2+} by external Na^+, we would expect that changing external Na^+ access to the permeation pathways should change the voltage dependence of Cd^{2+} modification. We tested this hypothesis by two approaches: First, we used extracellular Mg^{2+} to block permeation (Fig. S3). Consistent with our hypothesis, modification by internal Cd^{2+} became mostly voltage-insensitive at voltages where Mg^{2+} blockade was substantial (Fig. 5 *C*, *open diamonds*). However, it sharply changed at potentials where outwardly moving permeant ions effectively displaced the bound external Mg^{2+}. Second, we shifted the net flux of Na^+ along the voltage axis by reducing the external [Na^+] to 40 mM (Fig. S5). As expected, the entire voltage dependence of modification shifted leftward along the voltage axis (Fig. 5 *D*). Combined, these results strongly suggest that the voltage dependence of chemical modification by internal Cd^{2+} at the internal entryway of the selectivity filter (position T360C) results from incoming Na^+ expelling Cd^{2+} from the permeation pathway before modification can occur. Interestingly, the solid line in Fig. 5 *B* represents a fit of the modification data to a Boltzmann function. The steepness is consistent with one equivalent charge moving from the external bulk solution to the site occupied by Cd^{2+}.

A homology model of the voltage profile along an open CNG channel

The profile of the transmembrane potential along the axis of the channel was calculated using the PB-V equation (15) based on an atomic homology model of the CNG channel in the open conformation (Fig. 6 *A*). In Fig. 6 *B*, the ordinate represents the fraction of the transmembrane potential and the abscissa corresponds to the axis of the pore. The center of the bilayer is located at $z = 0$ Å. Consequently, the selectivity filter (TTIGET) is located between $z = 0.8$ and $z = 16.1$ (measured from the carbonyl oxygens of positions T359 and T364). The fraction of the total transmembrane potential measured at the side chains of positions T360 and T364 is 0.17 and 1, respectively. As with the experimental data, these calculations predict that most of the transmembrane voltage drops along the selectivity filter.

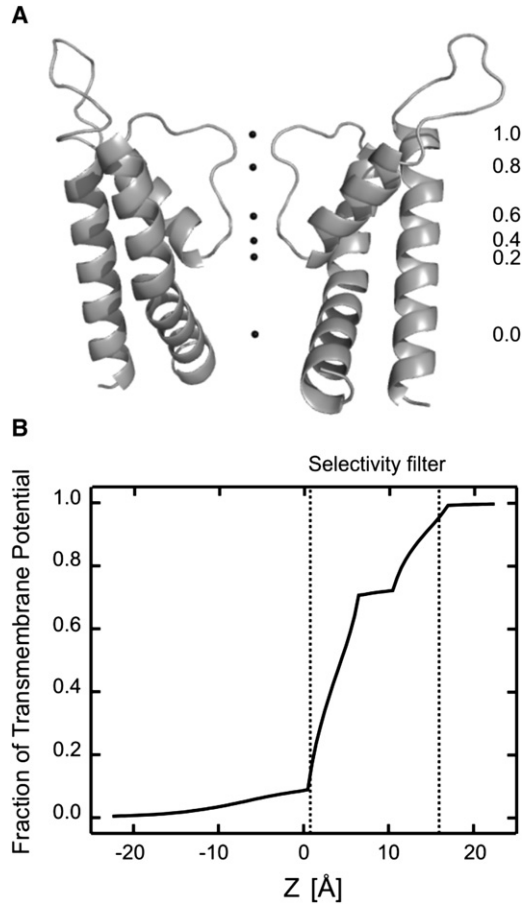

FIGURE 6 Fractional transmembrane potential along the axis of an open CNG channel pore. (*A*) Values of the fractional transmembrane potential are indicated along the permeation pathway of the CNG channel homology model. (*B*) The curve represents the profile of the potential along the pore of an open CNG channel homology model. The curve is drawn relative to extracellular solution which is assumed to have a value of 1. The selectivity filter is shown in dotted lines between $z = 0.8$ and $z = 16.1$.

DISCUSSION

Our functional studies indicate that the voltage drop along an open CNG channel is focused within the selectivity filter. We showed that modification of cysteine residues located in the middle of the intracellular cavity, or at the inner-facing end of the selectivity filter, by intracellularly applied charged probes did not show any direct voltage dependence. However, modification of cysteine residues located at the external end of the selectivity filter by intracellularly applied Ag^+ exhibited pronounced voltage dependence. Consistent with these data, theoretical calculations using a modified PB equation on a homology model of an open CNG channel showed a weak voltage drop along the inner cavity, and most of the transmembrane potential focused at the selectivity filter.

Quantitatively, our two approaches show remarkable agreement. Experimentally, the voltage dependence of internally applied Ag^+ modification at position T364C is consistent with a single charge traversing the complete transmembrane potential. By modeling, continuum electrostatic calculations indicate that the transmembrane potential drop at the side chain of position 364C is ~1 (i.e., the entire voltage drop along the permeation pathway). For positions located at the inner end of the selectivity filter, or at the middle of the intracellular cavity, our modification data

showed no detectable voltage dependence. Again, these results are consistent with continuum calculations which predict a mere 15% of the voltage drop along the intracellular cavity. These results combined, strongly suggest that the transmembrane potential in an open channel is indeed focused across the narrowest part of the permeation pathway, the selectivity filter. Using a purely theoretically approach, this has been predicted for many open channel structures or homology models of them (11,12). Modification data at position T364C also suggest that Ag^+, while passing through the selectivity filter, interacts little with other permeant ions. This result is not so surprising. As long as ions move in a concerted fashion, strong ion-ion interactions would be easily detected using electrophysiological methods, as they have been observed in K^+ channels (13). In CNG channels, on the other hand, many types of permeant ions show no apparent interaction between them (43–45), yet for other types of ions, ion-ion interactions are readily observed (46,47).

In contrast to Ag^+, modification by Cd^{2+} at the inner end of the selectivity filter (position T360C) showed strong voltage dependence. Where does this voltage dependence come from? We propose that it comes from external Na^+ permeating through the open channel and effectively competing with internal Cd^{2+} before modification occurs. In Fig. 5, we presented results from two sets of experiments that support this hypothesis. In both cases, reducing the translocation of external permeant ions drastically changed the voltage dependence of modification by Cd^{2+}. In addition, there is a long history of studies that describe how ion permeation affects the voltage dependence of internal blockers. For example, Armstrong and co-worker (21,48) showed that blockade of squid Kv channels by intracellular quaternary ammonium is voltage-dependent, and influenced by external K^+. They found that external K^+ increased TEA's rate of dissociation most significantly at membrane potentials that favored inward currents. Based on these findings, they hypothesized that the voltage dependence of blockade originates from external permeant ions moving across the transmembrane voltage and interacting with the blockers inside of the pore. Furthermore, recent reports on inward rectifying K^+ channels show a sharp voltage dependence for polyamine blockade, with electrical distances between 3 and 5. To explain these values, it has been proposed that voltage-dependent block by polyamines results primarily from the displacement of multiple K^+ ions traversing the transmembrane electric field as the blocker reaches its binding site (25,49–55). Finally, CNG channels are also blocked by QA and polyamines in a voltage-dependent-manner (41,42,56). In both cases, voltage dependence of blockade may come from permeant ions traversing the field rather than the charge carried by the blocker. External Na^+ may in fact influence Ag^+ modification at the inner end of the selectivity filter (position T360C), but only over a voltage range beyond our experimental protocols. In fact, we did observe a consistent reduction of modification rates at −80 mV but poor patch stability prevented us from examining more negative potentials.

Even though ion permeation is influenced by many factors (1,12,13,19), focusing the field along the selectivity filter in an open channel will optimize the coupling between the movement of permeant ions within the filter and the electromotive driving force, and consequently setting ion access to the inner cavity to be the rate limiting step for permeation.

SUPPORTING MATERIAL

Five figures are available at http://www.biophysj.org/biophysj/supplemental/S0006-3495(10)01049-0.

The background CNGA1 cysteine-less construct was a gift from Dr. William Zagotta. In addition, we thank Joe Mindell and Kenton Swartz for helpful discussions, and Josh Rosenthal for carefully reading the manuscript.

J.E.C. was supported by a Ruth L. Kirschstein Postdoctoral Fellowship. This research was supported by the Intramural Research Program of the National Institutes of Health, National Institute of Neurological Disorders and Stroke. V.J., A.Y.L., and B.R. are supported by grant No. GM-62342 from the National Institutes of Health.

REFERENCES

1. Hille, B. 2001. Ion Channels of Excitable Membranes. Sinauer Associates, Sunderland, MA.
2. Läuger, P. 1991. Electrogenic Ion Pumps. Sinauer Associates, Sunderland, MA.
3. Neher, E., and B. Sakmann. 1976. Single-channel currents recorded from membrane of denervated frog muscle fibers. *Nature.* 260: 799–802.
4. Bernèche, S., and B. Roux. 2001. Energetics of ion conduction through the K^+ channel. *Nature.* 414:73–77.
5. Bernèche, S., and B. Roux. 2003. A microscopic view of ion conduction through the K^+ channel. *Proc. Natl. Acad. Sci. USA.* 100: 8644–8648.
6. Brelidze, T. I., X. Niu, and K. L. Magleby. 2003. A ring of eight conserved negatively charged amino acids doubles the conductance of BK channels and prevents inward rectification. *Proc. Natl. Acad. Sci. USA.* 100:9017–9022.
7. Carvacho, I., W. Gonzalez, …, R. Latorre. 2008. Intrinsic electrostatic potential in the BK channel pore: role in determining single channel conductance and block. *J. Gen. Physiol.* 131:147–161.
8. D'Avanzo, N., H. C. Cho, …, P. H. Backx. 2005. Conduction through the inward rectifier potassium channel, Kir2.1, is increased by negatively charged extracellular residues. *J. Gen. Physiol.* 125:493–503.
9. Doyle, D. A., J. Morais Cabral, …, R. MacKinnon. 1998. The structure of the potassium channel: molecular basis of K^+ conduction and selectivity. *Science (NY).* 280:69–77.
10. Imoto, K., C. Busch, …, S. Numa. 1988. Rings of negatively charged amino acids determine the acetylcholine receptor channel conductance. *Nature.* 335:645–648.
11. Jiang, Y., A. Lee, …, R. MacKinnon. 2002. The open pore conformation of potassium channels. *Nature.* 417:523–526.
12. Jogini, V., and B. Roux. 2005. Electrostatics of the intracellular vestibule of K^+ channels. *J. Mol. Biol.* 354:272–288.

13. Morais-Cabral, J. H., Y. Zhou, and R. MacKinnon. 2001. Energetic optimization of ion conduction rate by the K^+ selectivity filter. *Nature.* 414:37–42.

14. Nimigean, C. M., J. S. Chappie, and C. Miller. 2003. Electrostatic tuning of ion conductance in potassium channels. *Biochemistry.* 42:9263–9268.

15. Roux, B. 1997. Influence of the membrane potential on the free energy of an intrinsic protein. *Biophys. J.* 73:2980–2989.

16. Roux, B., and R. MacKinnon. 1999. The cavity and pore helices in the KcsA K^+ channel: electrostatic stabilization of monovalent cations. *Science (NY).* 285:100–102.

17. Sobolevsky, A. I., M. V. Yelshansky, and L. P. Wollmuth. 2005. State-dependent changes in the electrostatic potential in the pore of a GluR channel. *Biophys. J.* 88:235–242.

18. Zhou, Y., and R. MacKinnon. 2003. The occupancy of ions in the K^+ selectivity filter: charge balance and coupling of ion binding to a protein conformational change underlie high conduction rates. *J. Mol. Biol.* 333:965–975.

19. Zhou, Y., J. H. Morais-Cabral, …, R. MacKinnon. 2001. Chemistry of ion coordination and hydration revealed by a K^+ channel-Fab complex at 2.0 Å resolution. *Nature.* 414:43–48.

20. Roux, B., S. Bernèche, and W. Im. 2000. Ion channels, permeation, and electrostatics: insight into the function of KcsA. *Biochemistry.* 39:13295–13306.

21. Armstrong, C. M. 1971. Interaction of tetraethylammonium ion derivatives with the potassium channels of giant axons. *J. Gen. Physiol.* 58:413–437.

22. Neyton, J., and C. Miller. 1988. Discrete Ba^{2+} block as a probe of ion occupancy and pore structure in the high-conductance Ca^{2+} -activated K^+ channel. *J. Gen. Physiol.* 92:569–586.

23. Neyton, J., and C. Miller. 1988. Potassium blocks barium permeation through a calcium-activated potassium channel. *J. Gen. Physiol.* 92:549–567.

24. Kutluay, E., B. Roux, and L. Heginbotham. 2005. Rapid intracellular TEA block of the KcsA potassium channel. *Biophys. J.* 88:1018–1029.

25. Lu, Z. 2004. Mechanism of rectification in inward-rectifier K^+ channels. *Annu. Rev. Physiol.* 66:103–129.

26. Contreras, J. E., D. Srikumar, and M. Holmgren. 2008. Gating at the selectivity filter in cyclic nucleotide-gated channels. *Proc. Natl. Acad. Sci. USA.* 105:3310–3314.

27. Shi, N., S. Ye, …, Y. Jiang. 2006. Atomic structure of a Na^+- and K^+-conducting channel. *Nature.* 440:570–574.

28. Alam, A., and Y. Jiang. 2009. High-resolution structure of the open NaK channel. *Nat. Struct. Mol. Biol.* 16:30–34.

29. Hamill, O. P., A. Marty, …, F. J. Sigworth. 1981. Improved patch-clamp techniques for high-resolution current recording from cells and cell-free membrane patches. *Pflugers Arch.* 391:85–100.

30. Canutescu, A. A., A. A. Shelenkov, and R. L. Dunbrack, Jr. 2003. A graph-theory algorithm for rapid protein side-chain prediction. *Protein Sci.* 12:2001–2014.

31. Fiser, A., and A. Sali. 2003. MODLOOP: automated modeling of loops in protein structures. *Bioinformatics.* 19:2500–2501.

32. Brooks, B. R., R. E. Bruccoleri, …, K. Martin. 1983. CHARMM: a program for macromolecular energy, minimization, and dynamics calculations. *J. Comput. Chem.* 4:187–217.

33. Im, W., D. Beglov, and B. Roux. 1998. Continuum solvation model: computation of electrostatics forces from numerical solutions to Poisson-Boltzmann equation. *Comput. Phys. Commun.* 111:59–75.

34. Akabas, M. H., D. A. Stauffer, …, A. Karlin. 1992. Acetylcholine receptor channel structure probed in cysteine-substitution mutants. *Science (NY).* 258:307–310.

35. Lu, Q., and C. Miller. 1995. Silver as a probe of pore-forming residues in a potassium channel. *Science (NY).* 268:304–307.

36. Yellen, G., D. Sodickson, …, M. E. Jurman. 1994. An engineered cysteine in the external mouth of a K^+ channel allows inactivation to be modulated by metal binding. *Biophys. J.* 66:1068–1075.

37. Benndorf, K., R. Koopmann, …, U. B. Kaupp. 1999. Gating by cyclic GMP and voltage in the alpha subunit of the cyclic GMP-gated channel from rod photoreceptors. *J. Gen. Physiol.* 114:477–490.

38. Eismann, E., F. Müller, …, U. B. Kaupp. 1994. A single negative charge within the pore region of a cGMP-gated channel controls rectification, Ca^{2+} blockage, and ionic selectivity. *Proc. Natl. Acad. Sci. USA.* 91:1109–1113.

39. Root, M. J., and R. MacKinnon. 1993. Identification of an external divalent cation-binding site in the pore of a cGMP-activated channel. *Neuron.* 11:459–466.

40. Armstrong, C. M. 1969. Inactivation of the potassium conductance and related phenomena caused by quaternary ammonium ion injection in squid axons. *J. Gen. Physiol.* 54:553–575.

41. Contreras, J. E., and M. Holmgren. 2006. Access of quaternary ammonium blockers to the internal pore of cyclic nucleotide-gated channels: implications for the location of the gate. *J. Gen. Physiol.* 127:481–494.

42. Guo, D., and Z. Lu. 2000. Mechanism of cGMP-gated channel block by intracellular polyamines. *J. Gen. Physiol.* 115:783–798.

43. Menini, A. 1990. Currents carried by monovalent cations through cyclic GMP-activated channels in excised patches from salamander rods. *J. Physiol.* 424:167–185.

44. Zimmerman, A. L., and D. A. Baylor. 1992. Cation interactions within the cyclic GMP-activated channel of retinal rods from the tiger salamander. *J. Physiol.* 449:759–783.

45. Frings, S., J. W. Lynch, and B. Lindemann. 1992. Properties of cyclic nucleotide-gated channels mediating olfactory transduction. Activation, selectivity, and blockage. *J. Gen. Physiol.* 100:45–67.

46. Furman, R. E., and J. C. Tanaka. 1990. Monovalent selectivity of the cyclic guanosine monophosphate-activated ion channel. *J. Gen. Physiol.* 96:57–82.

47. Qu, W., A. J. Moorhouse, …, P. H. Barry. 2001. Anomalous mole-fraction effects in recombinant and native cyclic nucleotide-gated channels in rat olfactory receptor neurons. *Proc. Biol. Sci.* 268: 1395–1403.

48. Armstrong, C. M., and L. Binstock. 1965. Anomalous rectification in the squid giant axon injected with tetraethylammonium chloride. *J. Gen. Physiol.* 48:859–872.

49. Guo, D., and Z. Lu. 2003. Interaction mechanisms between polyamines and IRK1 inward rectifier K^+ channels. *J. Gen. Physiol.* 122:485–500.

50. Guo, D., Y. Ramu, …, Z. Lu. 2003. Mechanism of rectification in inward-rectifier K^+ channels. *J. Gen. Physiol.* 121:261–275.

51. Guo, D., and Z. Lu. 2001. Kinetics of inward-rectifier K^+ channel block by quaternary alkylammonium ions. Dimension and properties of the inner pore. *J. Gen. Physiol.* 117:395–406.

52. Guo, D., and Z. Lu. 2000. Mechanism of IRK1 channel block by intracellular polyamines. *J. Gen. Physiol.* 115:799–814.

53. Shin, H. G., Y. Xu, and Z. Lu. 2005. Evidence for sequential ion-binding loci along the inner pore of the IRK1 inward-rectifier K^+ channel. *J. Gen. Physiol.* 126:123–135.

54. Shin, H. G., and Z. Lu. 2005. Mechanism of the voltage sensitivity of IRK1 inward-rectifier K^+ channel block by the polyamine spermine. *J. Gen. Physiol.* 125:413–426.

55. Xu, Y., H. G. Shin, …, Z. Lu. 2009. Physical determinants of strong voltage sensitivity of K^+ channel block. *Nat. Struct. Mol. Biol.* 16:1252–1258.

56. Martínez-François, J. R., and Z. Lu. 2010. Intrinsic versus extrinsic voltage sensitivity of blocker interaction with an ion channel pore. *J. Gen. Physiol.* 135:149–167.